Control of Iron Nitride Layers Growth Kinetics in the Binary Fe-N System

L. TORCHANE, P. BILGER, J. DULCY, and M. GANTOIS

This study is within the framework of a research program dedicated to defining the optimal conditions for the nitriding of iron and steels at atmospheric pressure by using various mixtures, NH_3-N_2-H_2 and NH_3-Ar. After studying the mechanisms of phase formation and mass transfer at the gas-solid interface, a mathematical model is developed in order to predict the nitrogen transfer rate in the solid, the nitride layer growth rate, and the nitrogen concentration profiles. In order to validate the model and to show its possibilities, it is compared with thermogravimetric experiments, analyses, and metallurgical observations (X-ray diffraction, optical microscopy, and electron microprobe analysis). The results obtained allow us to demonstrate the sound correlation between the experimental results and the theoretical predictions. By applying the model to the iron-nitrogen binary system, when the $\varepsilon/\gamma'/\alpha$ configuration referred to the Fe-N phase diagram is formed, we have experimentally determined the effective diffusion coefficient of nitrogen in the ε phase. The latter is constant for a composition of the ε nitride between 8 and 9.5 wt pct nitrogen. All the results obtained show that it is possible, by means of dynamic gas flow regulation, to eliminate the incubation period and to control the thickness, composition, and structure of the compound layer at the beginning of the treatment.

I. INTRODUCTION

NITRIDING and nitrocarburizing are thermochemical surface treatments of great importance in practice. They pronouncedly improve the surface quality (with respect to fatigue, corrosion, and wear).[1] There is a strong need for developing process control and automation techniques. Then, among other things, we should have available accurate models describing the kinetics and microstructural evolution of the iron nitride/iron nitrocarbonitride compound layer.

The control of iron nitride layer growth in the binary Fe-N system needs the gas-solid reaction to be monitored and the operating conditions which influence the total rate of the nitriding reaction to be defined.

At the first stages of nitriding, the transfer of nitrogen atoms from the gas phase (NH_3) to the solid (α-iron) occurs in the following steps:

(1) transport of ammonia in the gas phase and adsorption of molecules at the solid surface through a diffusion boundary layer;
(2) chemical reaction at the surface, which depends on the partial pressure;
(3) desorption of reaction products (N_2 and H_2), which depends on the total gas flow rate; and
(4) transfer of nitrogen atoms through the surface and diffusion into the material.

Each of these steps has its own specific kinetics which contribute to the global rate of the nitriding reaction. By definition, the slowest step determines the rate of the total process.[2–6] In this study, we are going to show that the diffusion in the solid state is the step that controls the process.

During our study, we have chosen operating conditions so that the transport of species in the gas phase and the chemical reaction on the surface do not impose a limitation on the reaction of nitriding.

So, for a given set of parameters (total gas flow rate and ammonia partial pressure), a surface nitrogen concentration can be fixed such that the ε, γ', and α phases are formed from the beginning of the treatment.[7] For this case, the reaction of nitriding is completely controlled by the kinetics of the layer growth governed by the diffusion laws in the solid state for a multiphase system.

Under these conditions, we are able to establish a diffusion model in the solid state, from the resolution of diffusion equations in a semi-infinite medium, and to predict the nitrogen transfer rate in the solid, as well as the nitride layer growth rate and the nitrogen concentration profiles.[8,9]

By means of thermogravimetry and dynamic gas flow rate regulation, we are able to show that it is possible to do the following.

(1) Determine experimentally the effective diffusion coefficient of nitrogen in the ε phase. This coefficient is compared to different values given in the literature.[10–13]
(2) Control over treatment time the thickness, composition, and structure of the compound layers.

The appropriate correlation between the model and the experiments is systematically validated by the micrographic measurement of the ε and γ' layer thicknesses and the precise determination of the surface nitrogen concentration by means of electron microprobe analysis.

II. GENERAL METHOD

The method used here is the following:

L. TORCHANE, Postdoctoral Fellow, P. BILGER, Graduate Student, J. DULCY, Research Engineer, and M. GANTOIS, Professor and Director, are with the Laboratory for Surface Science and Engineering, LSGS-URA CNRS 1402, Nancy School of Mines, 54042 Nancy Cedex, France.

Manuscript submitted July 5, 1995.

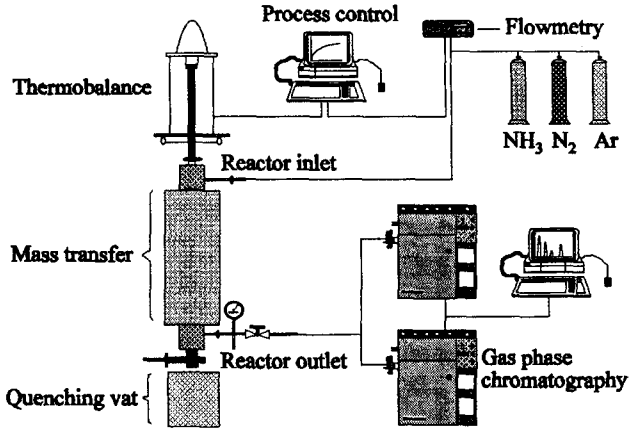

Fig. 1—Schematic representation of the instrumented thermogravimetry.

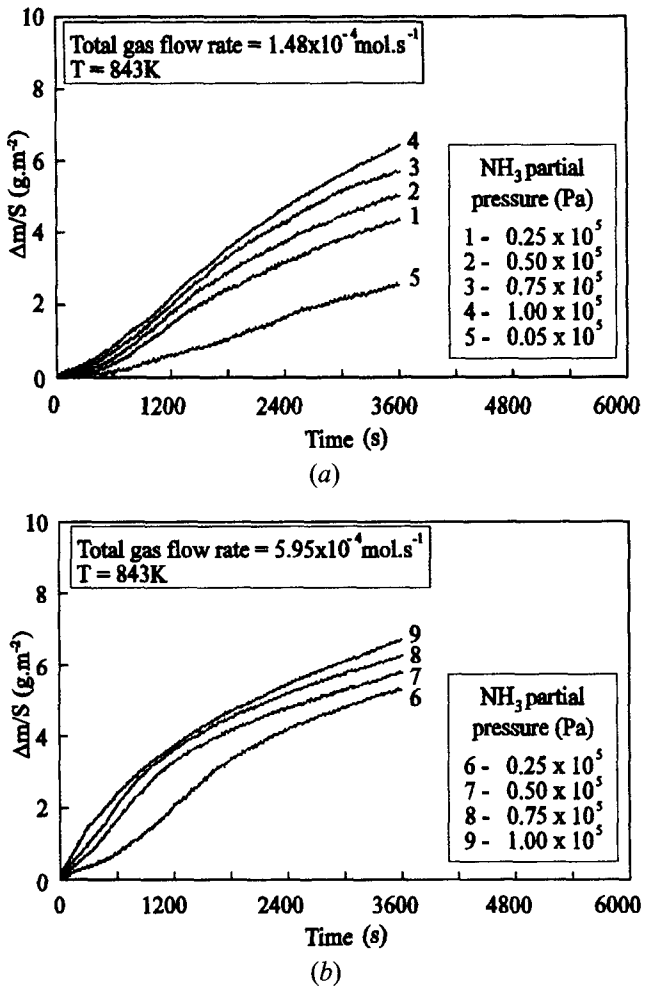

Fig. 2—Weight increase per unit area ($\Delta m/S$) as a function of nitriding time (t) for growth of an ε-Fe_2N_{1-y}/γ'-Fe_4N_{1-x} layer into a substrate α-Fe. Nitriding conditions: T = 843 K; total pressure 10^5 Pa ≅ 1 atm; and NH_3-N_2-H_2 total gas flow rate at the inlet of the reactor (*a*) 1.5×10^{-4} mol s^{-1} and (*b*) 6×10^{-4} mol s^{-1}.

(1) basic mass transfer mechanisms analysis;
(2) modeling of mass transfer in the solid and of the metallurgical microstructures;
(3) mass transfer monitoring from the data given by the model using thermogravimetric instrumentation; and
(4) metallurgical microstructure verification.

Metallurgical microstructures and the physicochemical surface study are determined by X-ray diffraction, optical microscopy, and electron microprobe analysis.

Instrumented thermogravimetry allows the testing of different hypotheses of the mass transfer model. A quenching device is used to determine the physicochemical and structural states of the samples. The set up is the following (Figure 1):

(1) thermobalance including an alumina cylindrical reactor with a special device for oil or water quenching,
(2) chromatographs allowing chemical species studies in the gas,
(3) mass flowmeters allowing the adjustment of the mass flow of each constituent of the gas phase in order to conduct the mass transfer in the sample according to the model laws,
(4) a computer allowing, on the one hand, acquisition and computation of the data and, on the other hand, the calculation of the mass transfer predicted by the model.

III. NITRIDING AT VARIABLE SURFACE NITROGEN CONCENTRATIONS

In order to know mechanisms of nitrogen transfer at the gas-solid interface and to study the influence of the gas composition on compound layer structure and growth, a large number of experiments have been performed at a temperature of 843 K during 1 hour periods at constant gas flow rates using NH_3-N_2-H_2 gas mixtures.

Figures 2(a) and (b) show some curves of mass variation obtained under the following conditions:[7] the NH_3-N_2-H_2 total gas flow rates used are 1.5×10^{-4} and 6×10^{-4} mol s^{-1}, and the ammonia partial pressures are 0.25, 0.50, 0.75, and 1 atm (1 atm ≅ 10^5 Pa). After nitriding, specimens are quenched in water.

The comparison of the two figures shows that the increase of the total gas flow rate increases the kinetics of the weight gain for a constant ammonia pressure. Moreover, for a fixed total gas flow rate, the weight increases with the time of treatment and the ammonia partial pressure. Therefore, if the total gas flow rate and the ammonia partial pressure increase, we can reduce the incubation period. The reaction of the nitriding is governed by two transfer phenomena at the surface: kinetic phenomena depending on the total flow rate and thermochemical phenomena depending on the partial pressure.

The light-microscopical analysis of the nitrided specimens (0.1 wt pct C) (Figures 3(a) and (b)) and the corresponding X-ray diffraction (Figures 4(a) and (b)) show that the ε/γ' ratio of ε and γ' phases is a function of the total gas flow rate, the ammonia partial pressure, and the time of the treatment. We can see (Figures 3(a) and (b)) that we obtained more ε and less γ' when the ammonia partial pressure increased.

Therefore, the total gas flow rate and ammonia partial pressure are, together with temperature, the fundamental parameters that control the treatment. If these parameters are kept constant during the treatment, it is impossible to control the ε and the γ' layer growth, because the surface nitrogen concentration is not constant during the treatment.

Consequently, controlling the surface metallurgical microstructures and the maximum treatment speed necessi-

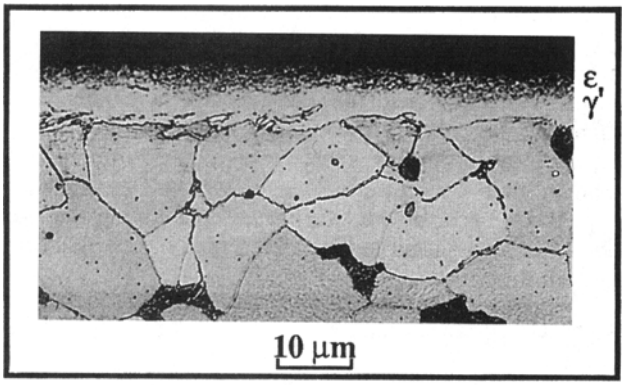

(*a*)

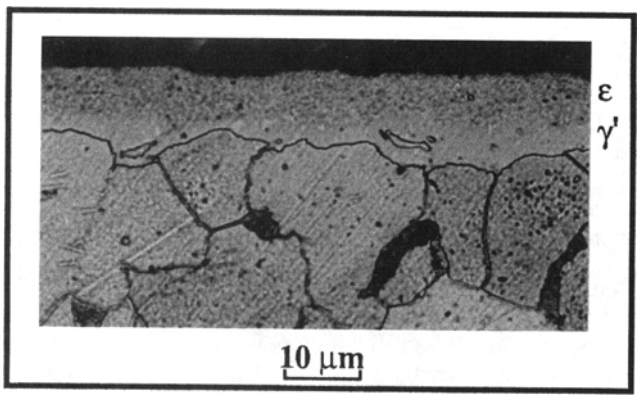

(*b*)

Fig. 3—Light-optical micrographs representing the evolution of the ε/γ' nitride layer after 1 h at 843 K. Nitriding conditions: NH_3-N_2-H_2 total gas flow rate at the inlet of the reactor 6×10^{-4} mol s^{-1} and ammonia partial pressure (*a*) 0.25×10^5 Pa and (*b*) 0.75×10^5 Pa.

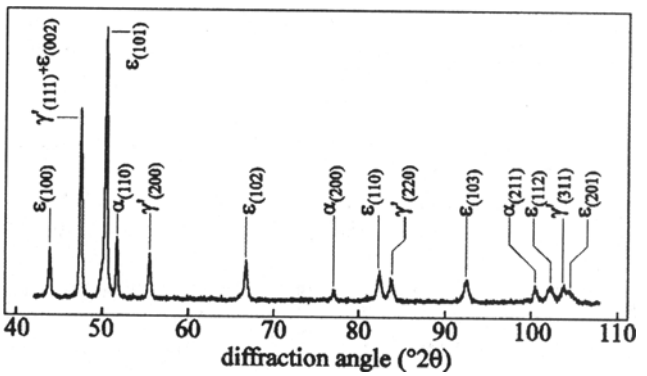

(*a*)

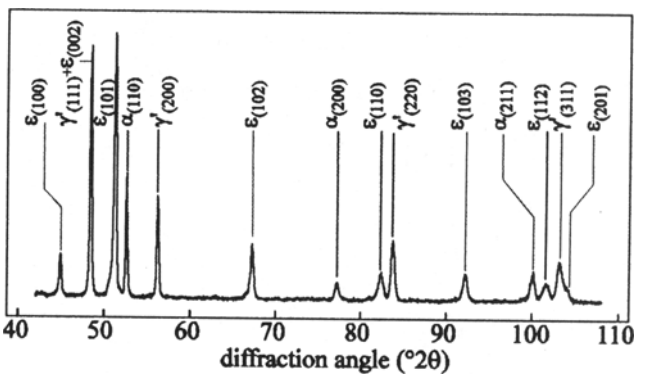

(*b*)

Fig. 4—X-ray diffractograms obtained from samples (0.1 wt pct C) nitrided for 1 h at 843 K. Nitriding conditions: NH_3-N_2-H_2 total gas flow rate at the inlet of the reactor 6×10^{-4} mol s^{-1} and ammonia partial pressure (*a*) 0.75×10^5 Pa and (*b*) 0.25×10^5 Pa.

tates, on the one hand, that the surface nitrogen concentration be fixed during the treatment and, on the other hand, that the reaction of nitriding be controlled by the diffusion laws in the solid state.

In the second part of this article, we are going to show that it is possible, by means of a mathematical model of layer growth (using the resolution of the diffusion equations of the Fe-N system), to control at the beginning of the treatment the formation and growth of the desired nitride layer configurations:

(1) nitrogen transfer in the α solid solution α-Fe
(2) nitrogen transfer in the biphase system α-Fe + γ'-Fe_4N_{1-x}
(3) nitrogen transfer in the triphase system α-Fe + γ'-Fe_4N_{1-x} + ε-Fe_2N_{1-y}

IV. MATHEMATICAL MODEL OF IRON NITRIDE LAYER GROWTH

The mathematical model is developed in order to predict the nitrogen transfer rate in the solid, the nitride layer growth rate, and the nitrogen concentration profiles. According to the binary Fe-N phase diagram (Figure 5),[14] only the nitrides γ'-Fe_4N_{1-x} and ε-Fe_2N_{1-y} can occur at usual nitriding temperatures and only a limited amount of nitrogen can be dissolved interstitially in the ferrite matrix (max. 0.4 at. pct at 863 K).

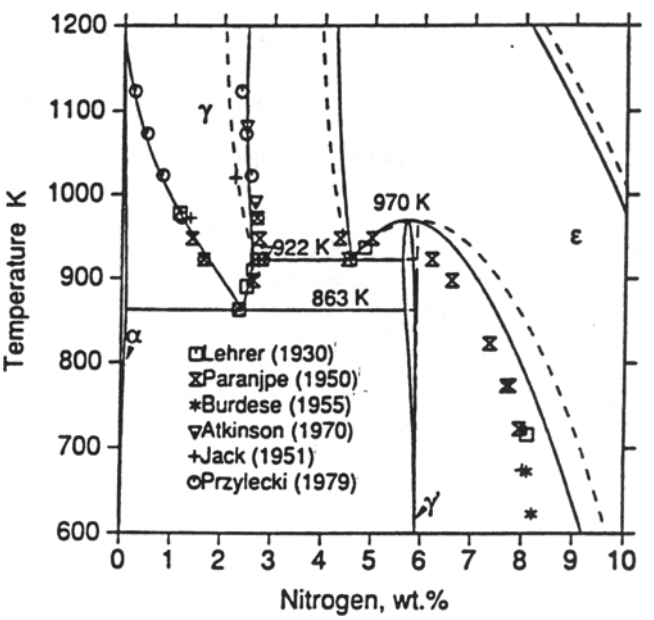

Fig. 5—Calculated Fe-N phase diagram together with experimental data on the phase boundaries.[15–20] Dashed lines are from the previous assessment.[21]

The surface region affected by nitriding can be subdivided in an adjacent surface compound layer consisting of γ' and ε nitrides and a diffusion zone underneath, where at the nitriding temperature, the nitrogen is dissolved in fer-

rite. Figure 6 shows the qualitative relation between the binary Fe-N phase diagram and the nitrogen concentration profiles for growth of a bilayer ε and γ' into a substrate α-Fe.

The kinetics of diffusion-controlled growth of the bilayer ε and γ' can be described by the shift of interfaces (ε/γ' and γ'/α) between ε, γ', and α because of a difference in the fluxes of nitrogen arriving at the interfaces and the fluxes of nitrogen being removed from the interfaces.[7,10,22] According to Fick's first law, the quantity of nitrogen that diffuses through the ε/γ' and γ'/α discontinuity planes during the time element dt is equal to the difference in diffusion fluxes (Figures 7 and 8). The equations used for shifting interfaces between ε, γ', and substrate α are established assuming that the diffusive flux of iron J^{Fe} in iron nitride is much smaller than that of nitrogen J^{N}.[23]

Nitrogen mass balance at the ε/γ' interface:

$$(C_{1\varepsilon\gamma'} - C_{2\varepsilon\gamma'}) \frac{d\lambda_\varepsilon}{dt} = \left[\left(-D_N^{(\varepsilon)} \frac{\partial C_\varepsilon(x,t)}{\partial x}\right)_{x=\lambda_\varepsilon} - \left(-D_N^{(\gamma')} \frac{\partial C_{\gamma'}(x,t)}{\partial x}\right)_{x=\lambda_\varepsilon}\right] \quad [1]$$

Nitrogen mass balance at the γ'/α interface:

$$(C_{1\gamma'\alpha} - C_{2\gamma'\alpha}) \frac{d\lambda_{\varepsilon\gamma'}}{dt} = \left[\left(-D_N^{(\gamma')} \frac{\partial C_{\gamma'}(x,t)}{\partial x}\right)_{x=\lambda_{\varepsilon\gamma'}} - \left(-D_N^{(\alpha)} \frac{\partial C_\alpha(x,t)}{\partial x}\right)_{x=\lambda_{\varepsilon\gamma'}}\right] \quad [2]$$

where

λ_ε and $\lambda_{\varepsilon\gamma'}$ are, respectively, the abscissas of the ε/γ' and γ'/α interfaces;

$\partial C_i(x, t)/\partial x$ is the nitrogen concentration gradient in the phase $i (i = \varepsilon, \gamma', \text{or } \alpha)$;

$d\lambda_\varepsilon/dt$ and $d\lambda_{\varepsilon\gamma'}/dt$ are the rates of interface advance;

$(C_{1\varepsilon\gamma'}, C_{2\varepsilon\gamma'})$ and $(C_{1\gamma\alpha}, C_{2\gamma\alpha})$ are, respectively, the nitrogen concentrations at the interfaces ε/γ' and γ'/α (equal to the equilibrium values from Fe-N phase diagram at 843 K); and

$D_N^{(\varepsilon)}$, $D_N^{(\gamma')}$, $D_N^{(\alpha)}$ are, respectively, the intrinsic diffusion coefficients of nitrogen in the ε, γ', and α phases.

As shown by Darken (1948)[24] and Schwerdtteger *et al.*,[23] the intrinsic diffusion coefficient can be expressed in terms of the (tracer) self-diffusivity D_N^* and the activity of the diffusing species (nitrogen); thus,

$$D_N^{(i)} = D_N^* \cdot \frac{d \ln a_N}{d \ln C_N} \quad [3]$$

where $d \ln a_N/d \ln C_N$ is the so-called thermodynamic factor.

Equation [3] shows that the intrinsic diffusion coefficient of nitrogen in phase i can be calculated from the corresponding self-diffusion coefficient if the dependence of the nitrogen activity a_N on the nitrogen concentration C_N is known.

At present, the diffusion coefficients of nitrogen in the nitrides ε and γ' are not known with sufficient accuracy. In the majority of the publications regarding this topic, a lack of data is apparent, in particular, the data related to the thermodynamic factor.[22,25,26] Therefore, in the present study, we have preferred to replace the intrinsic diffusion coefficients of nitrogen for ε and γ' layers with two effective diffusion coefficients defined recently by Somers and Mittemeijer[10] as the diffusion coefficients associated with the average diffusive fluxes through two layers of thickness λ_ε and $\lambda_{\gamma'}$ with concentration ranges (C_N^S to $C_{1\varepsilon\gamma'}$ and $C_{2\varepsilon\gamma'}$ to $C_{1\gamma\alpha}$), one each for the two phases constituting the two layers (phase ε adjacent to the surface and phase γ' adjacent to the substrate α).

For phase ε $(0 \le x \le \lambda_\varepsilon)$,

$$\langle D_N^{(\varepsilon)} \rangle = \frac{1}{C_N^S - C_{1\varepsilon\gamma'}} \cdot \int_{C_{1\varepsilon\gamma'}}^{C_N^S} D_N^{(\varepsilon)} \cdot dC_\varepsilon(x,t) \quad [4]$$

For phase γ' $(\lambda_\varepsilon \le x \le \lambda_{\varepsilon\gamma'})$,

$$\langle D_N^{(\gamma')} \rangle = \frac{1}{C_{2\varepsilon\gamma'} - C_{1\gamma'\alpha}} \cdot \int_{C_{1\gamma'\alpha}}^{C_{2\varepsilon\gamma'}} D_N^{(\gamma')} \cdot dC_{\gamma'}(x,t) \quad [5]$$

where

C_N^S is the surface nitrogen concentration at the initial interface for $x = 0$ (Figure 6).

Thus, the effective diffusion coefficients for the ε and γ' layers are taken as the average intrinsic diffusion coefficients through the thicknesses of the layers and are only dependent on temperature. This hypothesis has been verified experimentally for a semi-infinite system, and the results obtained show that the effective diffusion coefficient of nitrogen in the ε phase is constant for a composition of the ε nitride between 8 and 9.5 wt pct of nitrogen (*cf.*, Section V-E). The data used for the experimental determination of $\langle D_N^{(\varepsilon)} \rangle$ are given in the Appendix.

The effective diffusion coefficient obtained for the ε nitride sublayer at 843 K differs by a factor of 1.37 from the value calculated in Somers and Mittemeijer's[10] model. The approach used by these authors for the determination of effective diffusion coefficients of nitrogen in the ε and γ' phases is based on the evaluation of the self-diffusion coefficients of nitrogen and the thermodynamic factors (Eq. [3]).

In our case, the coefficient $\langle D_N^{(\varepsilon)} \rangle$ is determined graphically after the following steps.

(1) Replacing in Eqs. [1] and [2] $D_N^{(\varepsilon)}$, $D_N^{(\gamma')}$, and $D_N^{(\alpha)}$ with $\langle D_N^{(\varepsilon)} \rangle$, $\langle D_N^{(\gamma')} \rangle$, and $\langle D_N^{(\alpha)} \rangle$ so that at the ε/γ' interface,

$$(C_{1\varepsilon\gamma'} - C_{2\varepsilon\gamma'}) \cdot \frac{d\lambda_\varepsilon}{dt} = \left[\left(-\langle D_N^{(\varepsilon)} \rangle \cdot \frac{\partial C_\varepsilon(x,t)}{\partial x}\right)_{x=\lambda_\varepsilon} - \left(-\langle D_N^{(\gamma')} \rangle \cdot \frac{\partial C_{\gamma'}(x,t)}{\partial x}\right)_{x=\lambda_\varepsilon}\right] \quad [6]$$

and at the γ'/α interface,

$$(C_{1\gamma'\alpha} - C_{2\gamma'\alpha}) \cdot \frac{d\lambda_{\varepsilon\gamma'}}{dt} = \quad [7]$$

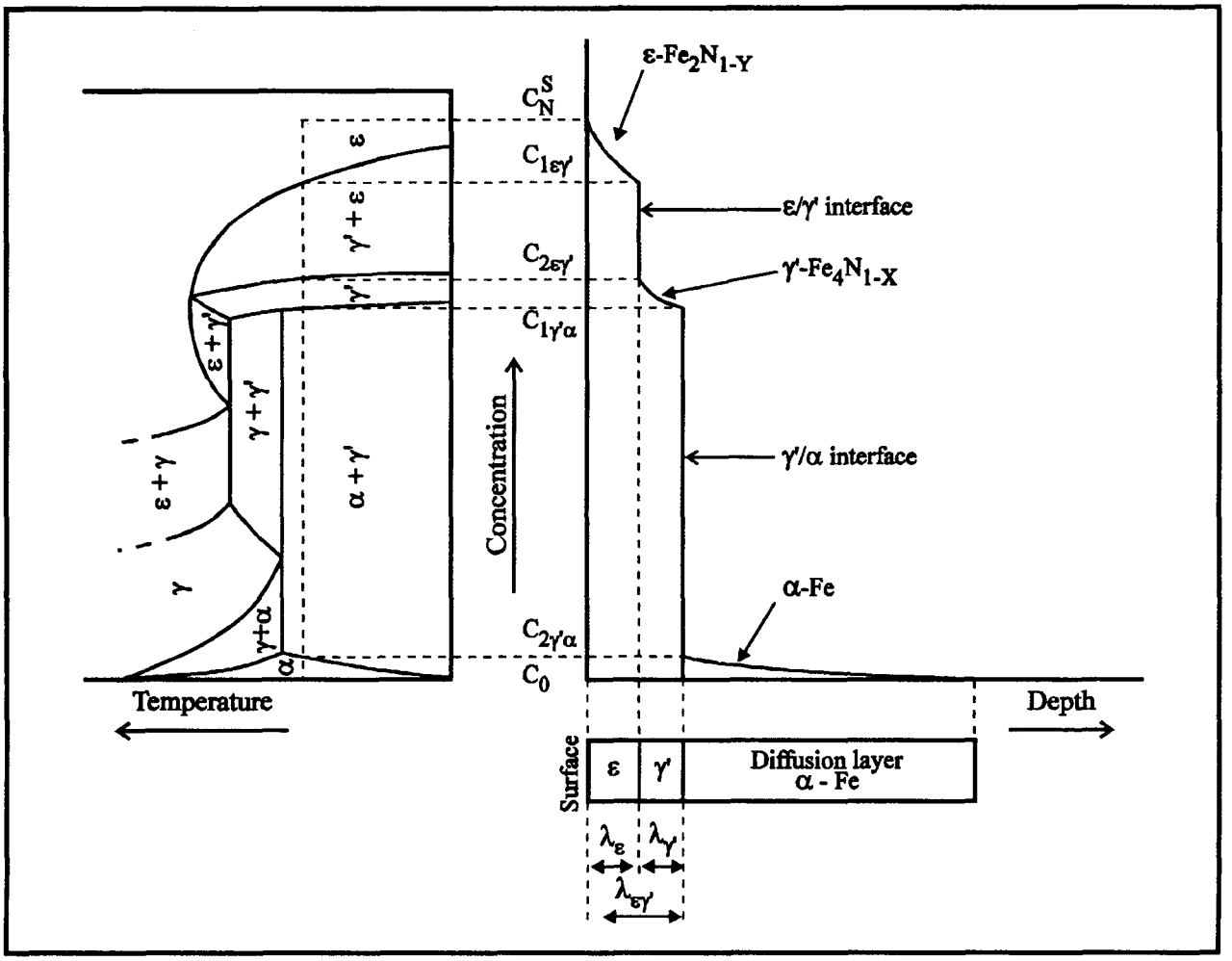

Fig. 6—Relation between the iron/nitrogen equilibrium diagram and concentration/depth for growth of a bilayer ε-Fe_2N_{1-y} and γ'-Fe_4N_{1-x} into a substrate α-Fe.

$$\left[\left(-\langle D_N^{(\gamma')}\rangle \cdot \frac{\partial C_{\gamma'}(x,t)}{\partial x}\right)_{x=\lambda_{\varepsilon\gamma'}} - \left(-\langle D_N^{(\alpha)}\rangle \cdot \frac{\partial C_{\alpha}(x,t)}{\partial x}\right)_{x=\lambda_{\varepsilon\gamma'}}\right]$$

(2) Solving Fick's second law (Eq. [8]), in order to know the nitrogen concentration gradient within the layers ε, γ', and α:

$$\frac{\partial C_i(x,t)}{\partial t} = \langle D_N^{(i)}\rangle \cdot \frac{\partial^2 C_i(x,t)}{\partial x^2} \qquad [8]$$

The solution of Eq. [8] for a semi-infinite medium relative to the formation of three phases ε, γ', and α can be formulated by the following expressions of nitrogen concentration profiles:[27,28]

$$C_\varepsilon(x,t) = A_\varepsilon + B_\varepsilon \cdot \mathrm{erf}\left(\frac{x}{2\sqrt{\langle D_N^{(\varepsilon)}\rangle \cdot t}}\right) \quad (0 \le x \le \lambda_\varepsilon) \qquad [9]$$

$$C_{\gamma'}(x,t) = A_{\gamma'} + B_{\gamma'} \cdot \mathrm{erf}\left(\frac{x}{2\sqrt{\langle D_N^{(\gamma')}\rangle \cdot t}}\right) \quad (\lambda_\varepsilon \le x \le \lambda_{\varepsilon\gamma'}) \qquad [10]$$

$$C_\alpha(x,t) = A_\alpha + B_\alpha \cdot \mathrm{erfc}\left(\frac{x}{2\sqrt{\langle D_N^{(\alpha)}\rangle \cdot t}}\right) \quad (\lambda_{\varepsilon\gamma'} \le x \le \infty) \qquad [11]$$

The constants A_ε, B_ε, $A_{\gamma'}$, $B_{\gamma'}$, A_α, and B_α used in Eqs. [9] through [11] are determined using the following boundary conditions.

(1) The model is applied for the nitriding of pure iron:

$$\text{for } t = 0 \text{ and } x > 0 \Rightarrow C(x,0) = C_0 = 0$$

where C_0 is the initial nitrogen concentration in the substrate.

(2) The effective diffusion coefficients of nitrogen in the ε and γ' phases are constant and independent of concentration for a composition of the ε nitride between 8 and 9.5 wt pct nitrogen.

(3) Local equilibrium at phase interfaces ε/γ' and γ'/α. This assumption implies that, on the one hand, the growth rate is given by the rate of diffusion through the layers ε and γ' and, on the other hand, the compositions at the ε/γ' and γ'/α interfaces are constant and independent of the time of treatment.

ε/γ' interface:

$$\text{for } t > 0 \text{ and } x = \lambda_\varepsilon \Rightarrow C_\varepsilon(\lambda_\varepsilon,t) = C_{1\varepsilon\gamma'} \text{ and } C_{\gamma'}(\lambda_\varepsilon,t) = C_{2\varepsilon\gamma'}$$

γ'/α interface:

$$\text{for } t > 0 \text{ and } x = \lambda_{\varepsilon\gamma'} \Rightarrow C_{\gamma'}(\lambda_{\varepsilon\gamma'},t) = C_{1\gamma'\alpha} \text{ and } C_\alpha(\lambda_{\varepsilon\gamma'},t) = C_{2\gamma'\alpha}$$

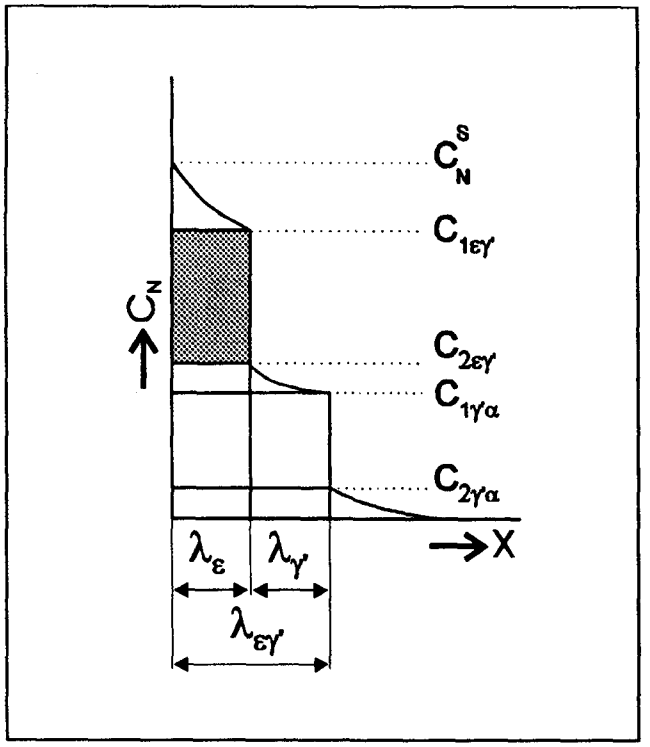

Fig. 7—Schematic concentration-depth profile for diffusion-controlled growth of a bilayer ε and γ'. The dark gray area indicates the amount of nitrogen that needs to be accumulated in the phase ε for shifting the interface between phases ε and γ' by a distance λ_ε to illustrate Eq. [1].

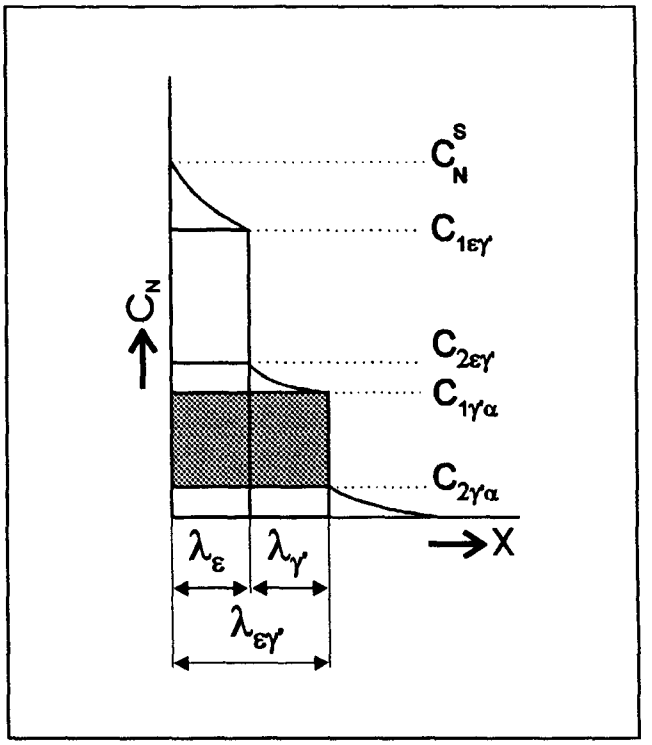

Fig. 8—Schematic concentration-depth profile for diffusion-controlled growth of a bilayer ε and γ'. The dark gray area indicates the amount of nitrogen that needs to be accumulated in the phase γ' for shifting the interface between phases γ' and α by a distance $\lambda_{\gamma'}$ to illustrate Eq. [2].

The boundary concentrations ($C_{1\varepsilon\gamma'}$, $C_{2\varepsilon\gamma'}$) and ($C_{1\gamma'\alpha}$, $C_{2\gamma'\alpha}$) are determined at a given temperature from the iron nitrogen phase diagram (Figure 6).

(4) The surface nitrogen concentration C_N^S is constant and controlled from the beginning of the treatment (the gas flow rate introduced in the reactor at $t = 0$ determines the nitrogen concentration at the surface of the ε nitride sublayer):

$$\text{for } t > 0 \text{ and } x = 0 \Rightarrow C_\varepsilon(0,t) = C_N^S$$

This hypothesis requires that both phases ε and γ' be formed instantaneously at $t = 0$. We have verified this condition experimentally by many experiments carried out at 843 K for 1 to 5 minutes on pure iron specimens.[7] After nitriding, the samples were cooled in water in order to avoid the transformations ($\varepsilon \rightarrow \gamma'$) and ($\gamma' \rightarrow \alpha$) during cooling. The X-ray diffraction patterns (Figure 9) allow us to confirm that both phases ε and γ' are formed after 5 minutes of treatment.

(5) The growth of the ε and γ' layers is a function of the square root of time:

$$\varepsilon \text{ layer for } 0 \le x \le \lambda_\varepsilon \Rightarrow \lambda_\varepsilon = b_\varepsilon \cdot \sqrt{t} \quad [12]$$

$$\varepsilon + \gamma' \text{ layers for } 0 \le x \le \lambda_{\varepsilon\gamma'} \Rightarrow \lambda_{\varepsilon\gamma'} = b_{\varepsilon\gamma'} \cdot \sqrt{t} \quad [13]$$

where b_ε and $b_{\varepsilon\gamma'}$ are the parabolic growth constants dependent on the surface nitrogen concentration imposed during the treatment, the phase compositions at the ε/γ' and γ'/α interfaces at a given temperature, and the effective diffusion coefficients of nitrogen in the ε, γ', and α phases.

This hypothesis has also been validated experimentally. Results obtained match the theoretical values calculated by Eqs. [12] and [13] (*cf.*, Section V–D).

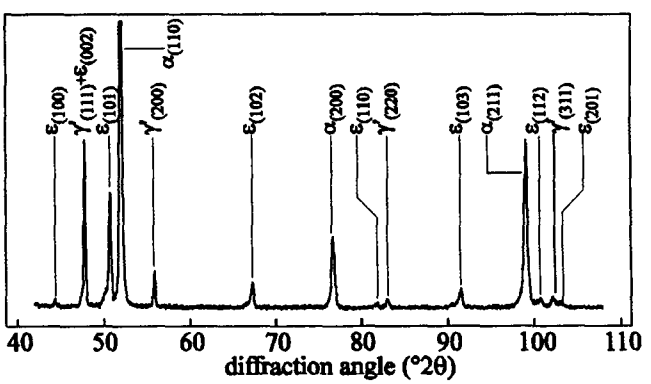

Fig. 9—X-ray diffractogram for growth of a bilayer ε-Fe_2N_{1-y} and γ'-Fe_4N_{1-x} into a substrate α-Fe obtained from pure iron nitrided for 5 min at 843 K and quenched in water. Nitriding conditions: ammonia partial pressure 10^5 Pa; NH_3 gas flow rate at the inlet of the reactor 7.44×10^{-4} mol s^{-1}; and surface nitrogen concentration at $t \ge 0$ $C_N^S = 10.50$ wt pct.

With the assumed boundary conditions, the nitrogen concentration profiles in the ε, γ', and α phases can be expressed as follows:

$$C_\varepsilon(x,t) = C_N^S + (C_{1\varepsilon\gamma'} - C_N^S) \cdot \frac{\operatorname{erf}\left(\frac{x}{2\sqrt{\langle D_N^{(\varepsilon)}\rangle \cdot t}}\right)}{\operatorname{erf}\left(\frac{b_\varepsilon}{2\sqrt{\langle D_N^{(\varepsilon)}\rangle}}\right)} \quad (0 \le x \le \lambda_\varepsilon) \quad [14]$$

$$C_{\gamma'}(x,t) = C_{2\varepsilon\gamma'}$$

$$\left\{\frac{\operatorname{erf}\left(\frac{b_{\varepsilon\gamma'}}{2\sqrt{\langle D_N^{(\gamma')}\rangle}}\right)-\operatorname{erf}\left(\frac{x}{2\sqrt{\langle D_N^{(\gamma')}\rangle\cdot t}}\right)}{\operatorname{erf}\left(\frac{b_{\varepsilon\gamma'}}{2\sqrt{\langle D_N^{(\gamma')}\rangle}}\right)-\operatorname{erf}\left(\frac{b_{\varepsilon}}{2\sqrt{\langle D_N^{(\gamma')}\rangle}}\right)}\right\}$$

$$-C_{1\gamma'\alpha} \qquad [15]$$

$$\left\{\frac{\operatorname{erf}\left(\frac{b_{\varepsilon}}{2\sqrt{\langle D_N^{(\gamma')}\rangle}}\right)-\operatorname{erf}\left(\frac{x}{2\sqrt{\langle D_N^{(\gamma')}\rangle\cdot t}}\right)}{\operatorname{erf}\left(\frac{b_{\varepsilon\gamma'}}{2\sqrt{\langle D_N^{(\gamma')}\rangle}}\right)-\operatorname{erf}\left(\frac{b_{\varepsilon}}{2\sqrt{\langle D_N^{(\gamma')}\rangle}}\right)}\right\} \quad (\lambda_\varepsilon \le x \le \lambda_{\varepsilon\gamma'})$$

$$C_\alpha(x, t) = C_{2\gamma'\alpha}$$

$$\left\{\frac{1-\operatorname{erf}\left(\frac{x}{2\sqrt{\langle D_N^{(\alpha)}\rangle\, t}}\right)}{1-\operatorname{erf}\left(\frac{b_{\varepsilon\gamma'}}{2\sqrt{\langle D_N^{(\alpha)}\rangle}}\right)}\right\} \quad (\lambda_{\varepsilon\gamma'} \le x \le \infty) \qquad [16]$$

After differentiating Eqs. [12] through [16] and substituting into Eqs. [6] and [7], we obtain

$$(C_N^S - C_{1\varepsilon\gamma'})\frac{\sqrt{\langle D_N^{(\varepsilon)}\rangle}\cdot\exp\left(\frac{-b_\varepsilon^2}{4\langle D_N^{(\varepsilon)}\rangle}\right)}{\operatorname{erf}\left(\frac{b_\varepsilon}{2\sqrt{\langle D_N^{(\varepsilon)}\rangle}}\right)} =$$

$$\frac{\sqrt{\pi}}{2}\cdot(C_{1\varepsilon\gamma'} - C_{2\varepsilon\gamma'})\cdot b_\varepsilon +$$

$$\frac{(C_{2\varepsilon\gamma'} - C_{1\gamma'\alpha})\cdot\sqrt{\langle D_N^{(\gamma')}\rangle}\cdot\exp\left(\frac{-b_\varepsilon^2}{4\langle D_N^{(\gamma')}\rangle}\right)}{\left[\operatorname{erf}\left(\frac{b_{\varepsilon\gamma'}}{2\sqrt{\langle D_N^{(\gamma')}\rangle}}\right)-\operatorname{erf}\left(\frac{b_\varepsilon}{2\sqrt{\langle D_N^{(\gamma')}\rangle}}\right)\right]} \qquad [17]$$

$$C_{2\gamma'\alpha}\frac{\sqrt{\langle D_N^{(\alpha)}\rangle}\cdot\exp\left(\frac{-b_{\varepsilon\gamma'}^2}{4\langle D_N^{(\alpha)}\rangle}\right)}{\left[1-\operatorname{erf}\left(\frac{b_{\varepsilon\gamma'}}{2\sqrt{\langle D_N^{(\alpha)}\rangle}}\right)\right]} =$$

$$-\frac{\sqrt{\pi}}{2}\cdot(C_{1\gamma'\alpha} - C_{2\gamma'\alpha})\cdot b_{\varepsilon\gamma'} +$$

$$\frac{(C_{2\varepsilon\gamma'} - C_{1\gamma'\alpha})\cdot\sqrt{\langle D_N^{(\gamma')}\rangle}\cdot\exp\left(\frac{-b_{\varepsilon\gamma'}^2}{4\langle D_N^{(\gamma')}\rangle}\right)}{\left[\operatorname{erf}\left(\frac{b_{\varepsilon\gamma'}}{2\sqrt{\langle D_N^{(\gamma')}\rangle}}\right)-\operatorname{erf}\left(\frac{b_\varepsilon}{2\sqrt{\langle D_N^{(\gamma')}\rangle}}\right)\right]} \qquad [18]$$

If we assume that the nitrogen surface concentration is constant during nitriding, we can determine constants b_ε and $b_{\varepsilon\gamma'}$ of Eqs. [17] and [18] graphically[8] (*cf.*, Appendix and Table VI).

Then, from expressions [12] through [16], we can deduce the nitrogen concentration profiles in the ε, γ', and α phases, the layer thicknesses, and the rates of interface advance resulting from the following relations:

$$V_{\varepsilon/\gamma'} = \frac{d\lambda_\varepsilon}{dt} = \frac{b_\varepsilon}{2\sqrt{t}} \qquad [19]$$

and

$$V_{\gamma'/\alpha} = \frac{d\lambda_{\varepsilon\gamma'}}{dt} = \frac{b_{\varepsilon\gamma'}}{2\sqrt{t}} \qquad [20]$$

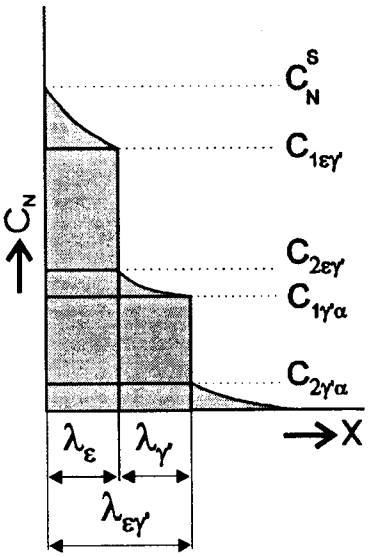

Fig. 10—Schematic concentration-depth profile for diffusion-controlled growth of a bilayer ε and γ'. The dark gray area indicates the total flux entering the layer at the surface S_L of the sample for $x = 0$ and $t \ge 0$.

According to Fick's first law, the total nitrogen mass that crosses the nitrided surface S_L of the sample at the instant t of treatment is (Figure 10),

$$M_{(\varepsilon,\gamma',\alpha)}(t) = S_L\int_0^t\left(J^N_{\varepsilon\gamma'}\right)_{x=0}\cdot dt$$

$$M_{(\varepsilon,\gamma',\alpha)}(t) = \frac{2S_L(C_N^S - C_{1\varepsilon\gamma'})}{\operatorname{erf}\left(\frac{b_\varepsilon}{2\sqrt{\langle D_N^{(\varepsilon)}\rangle}}\right)}\cdot\sqrt{\frac{\langle D_N^{(\varepsilon)}\rangle\cdot t}{\pi}} \qquad [21]$$

$$(C_N^S \ge C_{1\varepsilon\gamma'})$$

where $J^N_{\varepsilon\gamma'}$ is the flux of nitrogen entering the layer at the surface of the sample S_L.

For $x = 0$ and $t > 0$

$$\left(J^N_{\varepsilon\gamma'}\right)_{x=0} = -\langle D_N^{(\varepsilon)}\rangle\cdot\left(\frac{\partial C_\varepsilon(x, t)}{\partial x}\right)_{x=0} \qquad [22]$$

In the absence of the ε phase (or both ε and γ' phases), the total nitrogen mass is given by the following relations:

$$M_{(\gamma',\alpha)}(t) = S_L\int_0^t\left[-\langle D_N^{(\gamma')}\rangle\left(\frac{\partial C_{\gamma'}(x, t)}{\partial x}\right)_{x=0}\right]\cdot dt$$

$$M_{(\gamma',\alpha)}(t) = \frac{2S_L(C_N^S - C_{1\gamma'\alpha})}{\operatorname{erf}\left(\frac{b_{\varepsilon\gamma'}}{2\sqrt{\langle D_N^{(\gamma')}\rangle}}\right)}\cdot\sqrt{\frac{\langle D_N^{(\gamma')}\rangle\cdot t}{\pi}} \qquad [23]$$

$$(C_{1\gamma'\alpha} \le C_N^S \le C_{2\varepsilon\gamma'})$$

and

$$M_\alpha(t) = S_L\int_0^t\left[-\langle D_N^{(\alpha)}\rangle\left(\frac{\partial C_\alpha(x, t)}{\partial x}\right)_{x=0}\right]\cdot dt$$

$$M_\alpha(t) = 2S_L\cdot C_N^S\cdot\sqrt{\frac{\langle D_N^{(\alpha)}\rangle\cdot t}{\pi}} \quad (C_N^S = C_{2\gamma'\alpha}) \qquad [24]$$

Equations [21], [23], and [24] determine, for a given sur-

Table I. Comparison between the Experimental Value of the Effective Diffusion Coefficient of the Nitrogen in the ε Phase and the Data References (Activation Energy of Diffusion in Joule)

Effective Diffusion Coefficient of Nitrogen in the ε Phase ($m^2\ s^{-1}$)	References	Values of $<D_N^{(\varepsilon)}>$ at 843 K
$<D_N^{(\varepsilon)}> = 2.10 \times 10^{-8} \cdot \exp\left(\frac{-93,517}{RT}\right)$	Torchane[7]	3.40×10^{-14}
—	Somers and Mittemeijer[10]	4.65×10^{-14}
$<D_N^{(\varepsilon)}> = 4.43 \times 10^{-7} \cdot \exp\left(\frac{-113,177.2}{RT}\right)$	Du[11]	4.35×10^{-14}
$<D_N^{(\varepsilon)}> = 4.43 \times 10^{-7} \cdot \exp\left(\frac{-113,250}{RT}\right)$	Prenosil[12]	4.30×10^{-14}
$<D_N^{(\varepsilon)}> = 22.7 \times 10^{-6} \cdot \exp\left(\frac{-147,370}{RT}\right)$	Lakhtin and Kogan[13]	2.00×10^{-14}

face nitrogen concentration, the theoretical curves of the sample mass variation as a function of time.

V. COMPARISON OF EXPERIMENTAL RESULTS AND THEORETICAL PREDICTIONS

A. *Experimental Approach*

The principles of our approach are the following.

The mathematical model is established in order to calculate and predict the weight gain of the sample and the thicknesses of the layers as a function of time, the nature of the layers formed ($\varepsilon/\gamma'/\alpha$, γ'/α, or α), and the nitrogen concentration profiles in the ε, γ', and α, phases.

In order to study the layer growth kinetics, we perform thermogravimetric tests that consist of recording the weight gain of the samples as a function of time. During the treatment, we continuously adjust the gas flow rate at the inlet of the reactor in order to follow the theoretical curve of mass variation calculated by Eqs. [21], [23], and [24].

After treatment, the samples are quenched in water in order to avoid the transformations ($\varepsilon \rightarrow \gamma'$) and ($\gamma' \rightarrow \alpha$) during cooling. Metallurgical microstructures and the surface chemical study are determined by X-ray diffraction, optical microscopy, and electron microprobe analysis.

Experimental results obtained are compared with theoretical prediction.

B. *Experimental Determination of the Effective Diffusion Coefficient of Nitrogen in the ε Phase*

The experimental determination of the effective diffusion coefficient of nitrogen in the ε phase is based on the following principle.

Knowing the effective diffusion coefficients of nitrogen in the γ'[26] and α[29] phases and the relative evolution of the ε and γ' layer thicknesses when operating with a $\sqrt{t}$ law growth allows us to determine graphically the effective diffusion coefficient of nitrogen in the ε phase by Eqs. [17] and [18] after

(1) measuring the surface nitrogen concentration C_N^S by means of electron microprobe analysis and
(2) determining the parabolic growth constants b_ε and $b_{\varepsilon\gamma'}$ from the micrographic measurement of the layer thicknesses.

The evolution of the layer thicknesses as a function of temperature allows us to determine the frequency factor (D_N^0) and the activation energy of diffusion (E_a = 93,517 J).[7] So, the diffusion coefficient of nitrogen in the ε phase is

$$<D_N^{(\varepsilon)}> = D_N^0 \cdot \exp\left(\frac{-E_a}{RT}\right) = 2.1 \times 10^{-8} \cdot \exp\left(\frac{-93,517}{RT}\right) \quad (m^2\ s^{-1}) \quad [25]$$

In Table I, we can see that the effective diffusion coefficient of nitrogen obtained for the ε nitride at 843 K is in the range of the values given in the literature. These values differ by a factor of 1 to 2.

We think that this difference is due, on the one hand, to data used for the calculation of values for a diffusion coefficient of nitrogen in the ε nitride (particularly the nitrogen concentration at the ε/γ' and γ'/α interfaces) and, on the other hand, to experimental conditions used by these authors (temperature, gas mixture compositions, and chemical composition of the substrate).

A much higher energy was obtained by Lakhtin and Kogan.[13] However, their data were evaluated from plasma nitriding experiments. On the contrary, the data by Du[11] and Prenosil[12] are in satisfactory agreement with those obtained in the present work.

C. *Nitriding at Constant Surface Nitrogen Concentration*

The nitriding treatments are performed in a thermobalance furnace at atmospheric pressure on pure iron specimens (13 × 13 × 49 mm). We conducted the treatment by adjusting the reactor inlet gas flow rate in order to follow the theoretical curves of mass variation calculated by Eqs. [21], [23], and [24]. Figures 11(a), (b), and (c) show the experimental and theoretical weight gain of the samples per unit area ($\Delta m/S$) and the corresponding ammonia flow rate variation as a function of nitriding time (t) for

(1) growth of the ε-Fe_2N_{1-y}/γ'-Fe_4N_{1-x} layer into a substrate α-Fe − C_N^S = 8.50 wt pct,
(2) growth of the γ'-Fe_4N_{1-x} layer into a substrate α-Fe − C_N^S = 5.65 wt pct, and
(3) diffusion layer α-Fe − C_N^S = 0.08 wt pct.

We can see that the relative gas flow rate introduced in the reactor decreases regularly: it is very high at the beginning of the treatment to allow the immediate formation of the ε, γ', or α nitride, and it rapidly decreases to become very low at the end of the treatment.

The X-ray diffraction patterns (Figures 12(a) through (c)) and the optical microscopy images (Figures 13(a) and (b)) confirm the nature of the phases obtained.

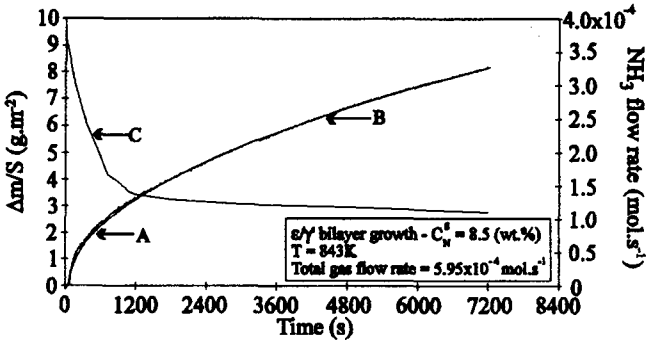

(*a*)

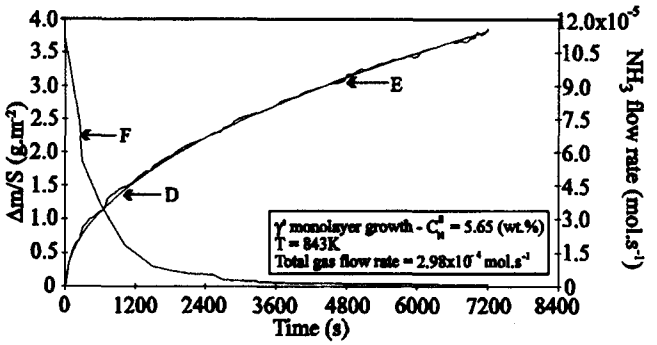

(*b*)

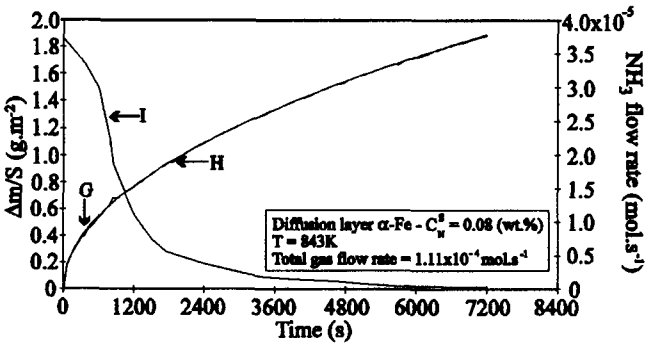

(*c*)

Fig. 11—Weight increase per unit area ($\Delta m/S$) and the corresponding ammonia flow rate variation as a function of nitriding time (t) for growth of (*a*) ε/γ' layer into a substrate α-C_N^s = 8.5 wt pct, (*b*) γ' layer into a substrate α-C_N^s = 5.65 wt pct, and (*c*) diffusion layer α-C_N^s = 0.08 wt pct. (A, D, and G) and (B, E, and H) are, respectively, the theoretical and experimental curves of the weight gain of the samples per unit area, and (C, F, and I) are the experimental curves of the ammonia flow rate variation.

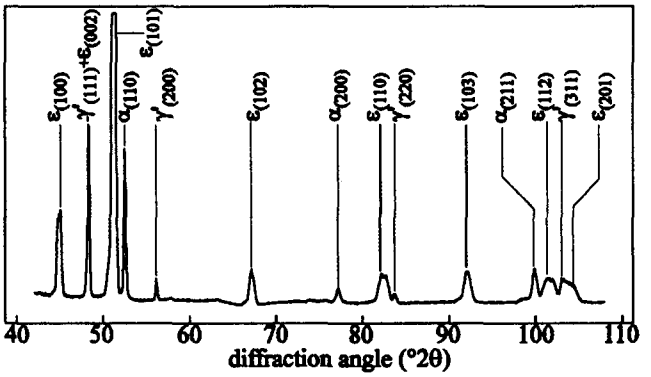

(*a*)

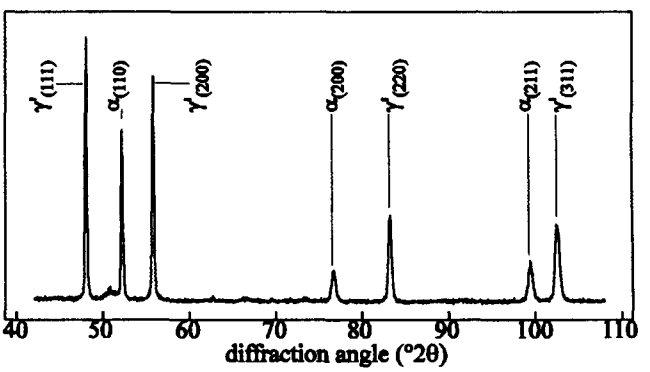

(*b*)

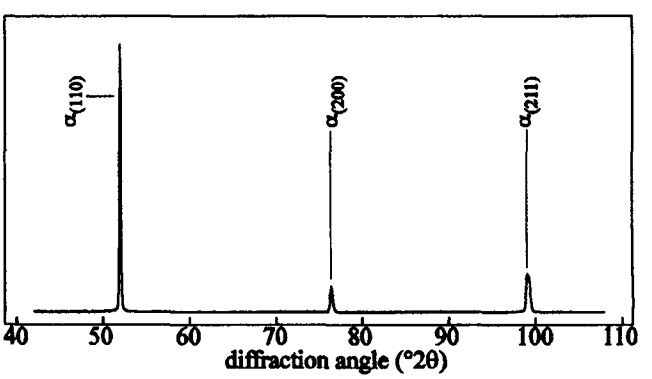

(*c*)

Fig. 12—X-ray diffractograms obtained from samples nitrided for 2 h at 843 K for growth of (*a*) ε/γ' layer into a substrate α-C_N^s = 8.50 wt pct, (*b*) γ' layer into a substrate α-C_N^s = 5.65 wt pct, and (*c*) diffusion layer α-C_N^s = 0.08 wt pct.

D. *Kinetics of ε and γ' Layers Growth*

The experimental study of ε and γ' layer growth is carried out at 843 K on pure iron specimens. The characteristic results of the micrographic measures of the layer thicknesses and of the quantitative analysis of the surface nitrogen concentration (Tables II and III) allow us to confirm, on the one hand, that the different tests were performed at constant surface nitrogen concentration and, on the other hand, the correspondence between the experimental and theoretical thicknesses of the layers.

The evolution of the layer thicknesses as a function of the square root of the diffusion time show (Figures 14(a) and (b)) that the layers' growth is parabolic. Therefore, the chemical equilibria at the ε/γ' and γ'/α interfaces are well established and the growth kinetics of the layers is controlled by diffusion.

E. *Validation of Model*

In order to determine the interval of nitrogen concentration in which the model is valid, we have performed many experiments of nitriding at 843 K for nitrogen concentrations between 8 and 9.5 wt pct. Figures 15 and 16 show, respectively, the experimental variation of the weight gain of the sample and the ammonia gas flow rate as a function of time and surface nitrogen concentration.

We can see (Figure 16) that for C_N^s = 8 wt pct, the ammonia gas flow rate introduced in the reactor decreases regularly: it is very high at the beginning of the treatment to allow the immediate formation of the ε nitride, and it

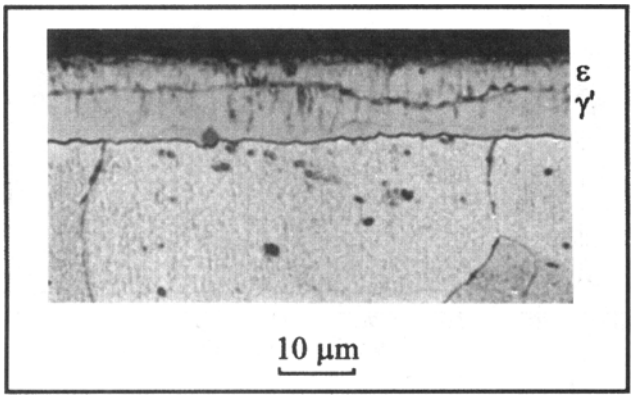

(*a*)

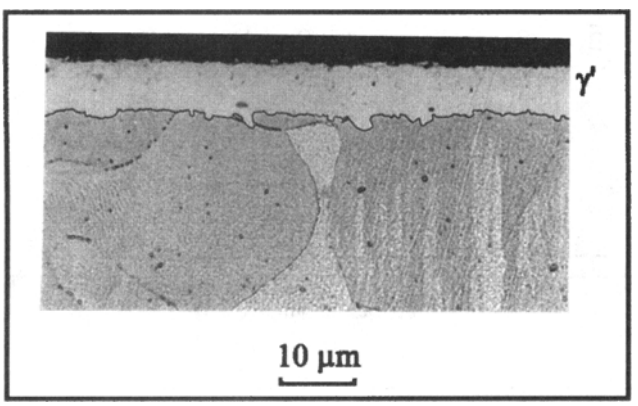

(*b*)

Fig. 13—Light-optical micrographs obtained from samples nitrided for 2 h at 843 K for growth of (*a*) ε/γ' layer into a substrate α-C_N^S = 8.50 wt pct and (*b*) γ' layer into a substrate α-C_N^S = 5.65 wt pct.

Table II. Experimental and Theoretical (in Bold) Thicknesses of the ε and γ' Layers and Surface Nitrogen Concentrations as a Function of the Nitriding Time for Growth of an ε-Fe_2N_{1-y}/γ'-Fe_4N_{1-x} Layer into a Substrate α-Fe (T = 843 K)

	Time of Treatment, t (Hours)				
	0.5	1	2	3	4
Surface nitrogen concentration, C_N^S (wt pct)	8.50	8.47	8.52	8.53	8.48
	8.50	**8.50**	**8.50**	**8.50**	**8.50**
(ε + γ') total layer thickness, $\lambda_{\varepsilon\gamma'}$ (μm)	6.00	8.50	12.20	14.80	17.10
	6.15	**8.70**	**12.30**	**15.07**	**17.40**
ε layer thickness, λ_ε (μm)	2.65	3.65	5.40	6.50	7.75
	2.69	**3.81**	**5.39**	**6.60**	**7.62**
γ' layer thickness, $\lambda_{\gamma'}$ = ($\lambda_{\varepsilon\gamma'} - \lambda_\varepsilon$) ($\mu$m)	3.35	4.85	6.80	8.30	9.35
	3.46	**4.89**	**6.91**	**8.47**	**9.78**

rapidly decreases to become very low at the end of the treatment.

On the contrary, for $C_N^S > 8$ wt pct, the experimental curve of the ammonia gas flow rate shows two inflection points (t_{min} and t_{max}). These extremes shift to a shorter treatment time when the surface nitrogen concentration increases.

(1) t_{min} shows the beginning of pore formation in the ε layer: the recombination of the nitrogen atoms results from the reaction $2N \rightarrow N_2$ [I].* For $t > t_{min}$, we have

Table III. Experimental and Theoretical (in Bold) Thicknesses of the γ' Layer and Surface Nitrogen Concentrations as a Function of the Nitriding Time for Growth of a γ'-Fe_4N_{1-x} Layer into a Substrate α-Fe (T = 843 K)

	Time of Treatment, t (Hours)				
	0.25	0.50	1	2	4
Surface nitrogen concentration, C_N^S (wt pct)	5.68	5.60	5.63	5.65	5.63
	5.65	**5.65**	**5.65**	**5.65**	**5.65**
γ' layer thickness, $\lambda_{\gamma'}$ (μm)	2.40	3.20	4.55	6.45	9.15
	2.34	**3.31**	**4.68**	**6.62**	**9.36**

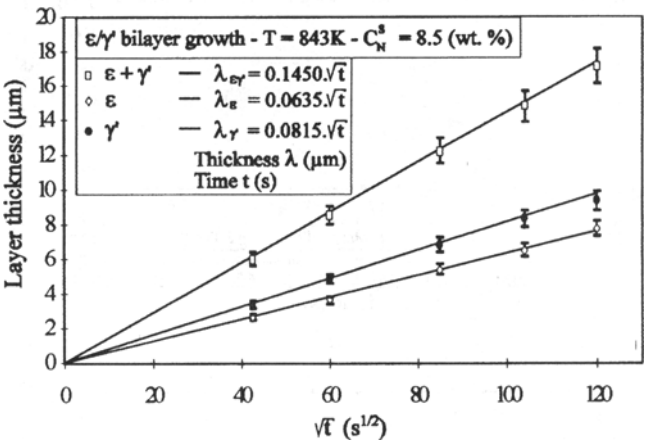

(*a*)

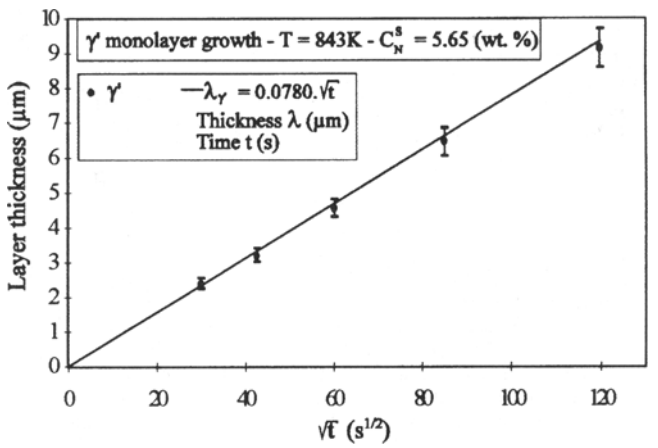

(*b*)

Fig. 14—Evolution of the layer thicknesses as a function of the square root of the nitriding time for growth of (*a*) ε/γ' layer into a substrate α-C_N^S = 8.50 wt pct and (*b*) γ' layer into a substrate α-C_N^S = 5.65 wt pct.

*Pore formation frequently occurs due to the extremely high pressure that results from reaction [I] if equilibrium is approached in a closed nucleus in the compound layer.[30] The partial pressure of nitrogen gas (N_2) in equilibrium with ε nitride amounts to about 250,000 atm.[31] As shown by Somers and Mittemeijer,[10] pore formation is observed especially in the near surface region because most nitrogen is present there. After prolonged nitriding, porosity also develops intragranularly. Coalescence of individual pores leads to the development of channels that connect the interior of the compound layer with the outer surface. These pore channels represent a very large surface area, leading to considerable denitriding *via* reaction [I].

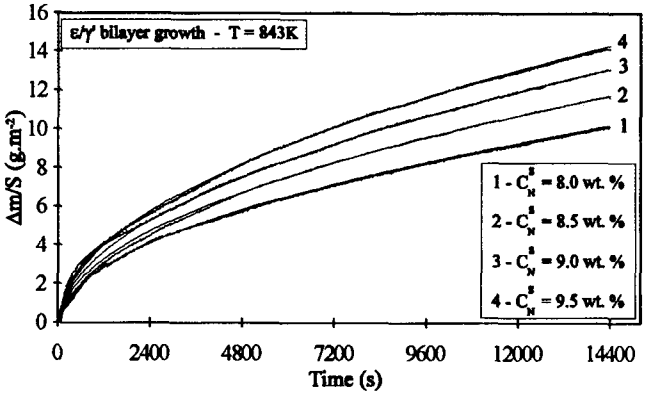

Fig. 15—Weight increase per unit area ($\Delta m/S$) as a function of nitriding time for growth of an ε/γ' layer into a substrate α. Nitriding conditions: T = 843 K; t = 4 h; and surface nitrogen concentration 1—C_N^S = 8.0, 2—C_N^S = 8.5, 3—C_N^S = 9.0, and 4—C_N^S = 9.5 (wt pct).

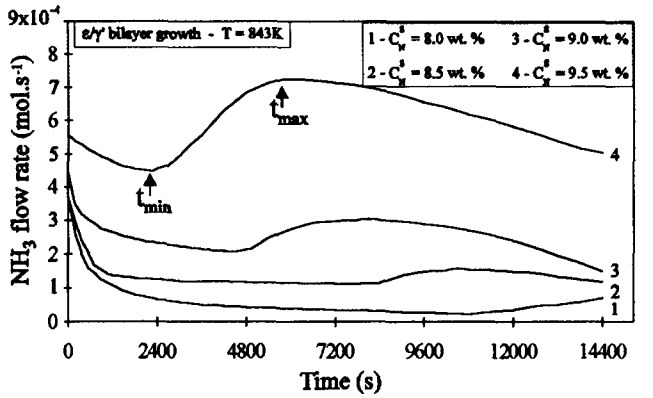

Fig. 16—Ammonia gas flow rate variation as a function of nitriding time and surface nitrogen concentration (C_N^S). Nitriding conditions: T = 843 K; t = 4 h; and surface nitrogen concentration: 1—C_N^S = 8.0, 2—C_N^S = 8.5, 3—C_N^S = 9.0, and 4—C_N^S = 9.5 (wt pct).

Table IV. Comparison between Experimental and Theoretical (in Bold) Values of the Surface Nitrogen Concentration and the Layer Thicknesses as a Function of the Surface Nitrogen Concentration and the Nitriding Time (T = 843 K and t = 4 Hours)

Surface nitrogen concentration, C_N^S (wt pct)	7.90	8.54	9.10	9.45
	8.00	**8.50**	**9.00**	**9.50**
(ε + γ') total layer thickness, $\lambda_{\varepsilon\gamma'}$ (μm)	15.70	17.10	18.85	20.85
	15.96	**17.40**	**19.08**	**20.76**
ε layer thickness, λ_ε (μm)	4.60	7.75	10.00	12.15
	4.92	**7.62**	**9.84**	**11.82**
γ' layer thickness, $\lambda_{\gamma'} = (\lambda_{\varepsilon\gamma'} - \lambda_\varepsilon)$ (μm)	11.10	9.35	8.85	8.70
	11.04	**9.78**	**9.24**	**8.94**

increased the ammonia partial pressure in the gas mixture at the inlet of the reactor in order to follow the calculated weight gain from the model and to maintain a constant nitrogen concentration at the surface of the sample.

(2) t_{max} shows the beginning of coalescence of individual pores and development of channels. Figure 16 shows that for $t > t_{max}$, the ammonia flow rate decreases regularly. This decrease is certainly due to the coalescence of pores and the development of channels.

The characteristic results of nitriding obtained by optical microscopy and electron microprobe analysis show (Table IV) that the model is validated in the nitrogen concentration interval 8 to 9.5 wt pct. The experimental measures of the surface nitrogen concentration and the thicknesses of the layers are comparable to those predicted by the model.

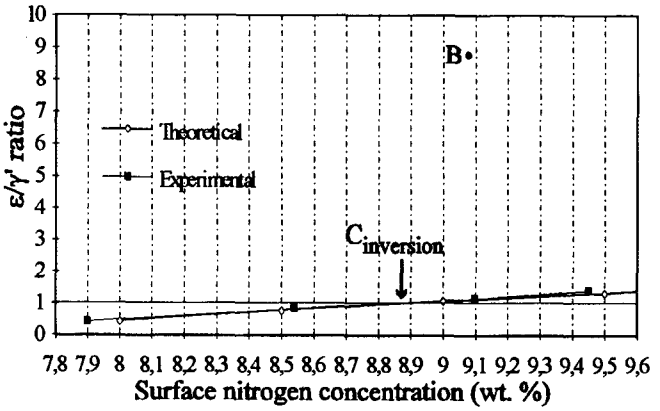

Fig. 17—Evolution of the experimental and theoretical ratio of the ε and γ' layer thicknesses as a function of the surface nitrogen concentration. Nitriding conditions: T = 843 K; t = 4 h; and surface nitrogen concentration (8.0 ÷ 9.5) (wt pct). The ε/γ' ratio is equal to one for $C_N^S = C_{inv}$ = 8.87 wt pct.

In Figure 17, we have shown the experimental and theoretical evolution of the ε/γ' ratio of the ε and γ' layer thicknesses as a function of the surface nitrogen concentration. We can see that the ε/γ' ratio increases appreciably when the surface nitrogen concentration increases. For C_N^S = 8.87 wt pct (noted $C_{inversion}$ on the curve), the ε/γ' ratio is equal to one, and for $C_N^S > 8.87$ wt pct, the ε layer is above that of layer γ'.

To arrive at these results, it was necessary to conduct the treatments by regularly adjusting the gas flow rate at the inlet of the reactor in order to follow the theoretical weight gain of the sample and to maintain a constant surface nitrogen concentration (Figure 17).

After several experiments performed at constant gas flow rate (ammonia pressure 10^5 Pa and ammonia gas flow rate 7.44×10^{-4} mol s^{-1}), we have shown the following.[7]

(1) On the one hand, for treatment times of 5 and 240 minutes, the surface nitrogen concentration varies, respectively, from 10.5 to 9.1 wt pct.
(2) On the other hand, the porosity has developed in the surface adjacent part of the ε nitride sublayer.

Consequently, the ε/γ' ratio of the ε and γ' layers is approximately equal to nine (for t = 240 minutes and C_N^S = 9.1 wt pct; *cf.*, Figure 17, point B). For a constant surface nitrogen concentration of 9.1 wt pct, the calculated ε/γ' ratio is 1.11 as compared to 9 when the surface nitrogen concentration varies over time.

All of these results undeniably show that it is important to control the evolution of the surface nitrogen concentration over time in order to control the porosity at the surface of the material and to prevent the disordered growth of compound layers in such a way as to use them industrially.

VI. CONCLUSIONS

The model has been developed in order to control the nitride layer growth kinetics in the Fe-N binary system.

After studying the mechanisms of phase formation and

mass transfer at the gas-solid interface, we have determined the operating conditions (total gas flow rate and ammonia partial pressure) so that the ε, γ', and α phases can be formed from the beginning of the treatment. So, the nitriding process is completely controlled by the kinetics of the layer growth governed by the diffusion laws in the solid state for a multiphase system.

In order to solve the diffusion equations in a semi-infinite medium and to predict the nitrogen transfer rate in the solid, the nitride layer growth rate, and the nitrogen concentration profiles, we have used the following assumptions.

(1) The local equilibrium at phase interfaces ε/γ' and γ'/α is maintained during nitriding.
(2) The surface nitrogen concentration is constant and controlled from the beginning of the treatment.
(3) The growth kinetics of the ε and γ' layers is parabolic.
(4) The effective diffusion coefficients of nitrogen in the ε and γ' phases are constant and independent of concentration. These coefficients are taken as the average intrinsic diffusion coefficients of nitrogen throughout the thicknesses of the layers ε and γ' and are only dependent on temperature.

All of these assumptions have been validated experimentally in the nitrogen concentration interval 8 to 9.5 wt pct. The value obtained for the effective diffusion coefficient of nitrogen in the ε nitride ($\langle D_N^{(\varepsilon)} \rangle$) is in good agreement with data taken from the literature. Applying the model to the Fe-N-C system, we have also shown that the expression of $\langle D_N^{(\varepsilon)} \rangle$ remains valid in the carbon + nitrogen concentration range 7 to 9.5 wt pct. The results obtained are in publication.

The trend is now oriented toward process automation and optimization. It is necessary to dispose of a diffusion model describing the layer growth kinetics and an experimental validation means. The results obtained allow us to think that this aim is achieved for the Fe-N and Fe-N-C systems, because these results demonstrate the possibility of eliminating the nitrogen transfer resistance at the gas-solid interface and of controlling the thickness, composition, and structure of the compound layers over treatment time.

APPENDIX
Data used for the experimental determination of the effective diffusion coefficient in the ε phase

(1) Composition at phase boundaries (Table AI and Figures A1 through A3).
(2) Graphical solution of Eqs. [17] and [18][7] (Table AII).
(3) Effective diffusion coefficients of nitrogen in the ε, γ', and α phases.

$$\langle D_N^{(\varepsilon)} \rangle = 2.100 \times 10^{-08} \cdot \exp\left(\frac{-93{,}517\ [7]}{RT}\right) \quad (m^2\ s^{-1})$$

$$\langle D_N^{(\gamma')} \rangle = 1.675 \times 10^{-09} \cdot \exp\left(\frac{-64{,}000\ [26]}{RT}\right) \quad (m^2\ s^{-1})$$

$$\langle D_N^{(\alpha)} \rangle = 6.600 \times 10^{-07} \cdot \exp\left(\frac{-77{,}900\ [29]}{RT}\right) \quad (m^2\ s^{-1})$$

$$R = 8.32 \quad (J\ K^{-1}\ mol^{-1})$$

(4) The calculated relative variation of the surface nitrogen concentration and the ε and γ' layer thicknesses (Table AIII).

Table AI. Composition at Phase Boundaries*

Position		N Content (Wt Pct) Calculated at 843 K[7]	N Content (Wt Pct) Calculated at 843 K[10]
ε/γ' interface	$C_{1\varepsilon\gamma'}$	(7.35)	7.16
	$C_{2\varepsilon\gamma'}$	(5.75)	5.85
γ'/α interface	$C_{1\gamma'\alpha}$	(5.50)	5.70
	$C_{2\gamma'\alpha}$	(0.08)	0.09

*The values in parentheses are obtained by interpolation of the data by Paranjpe et al.[16]

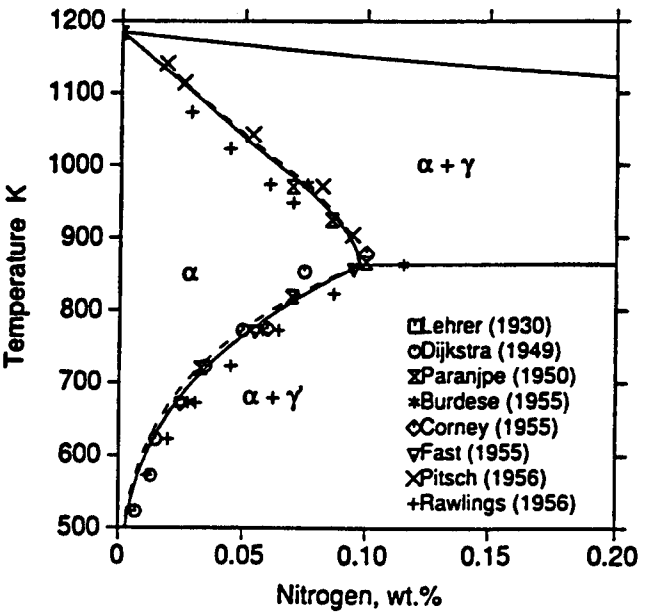

Fig. A1—Part of the calculated Fe-N phase diagram showing the α-phase boundary together with experimental data[15–17,32–26] and the previous description by Frisk[21] (dashed lines).

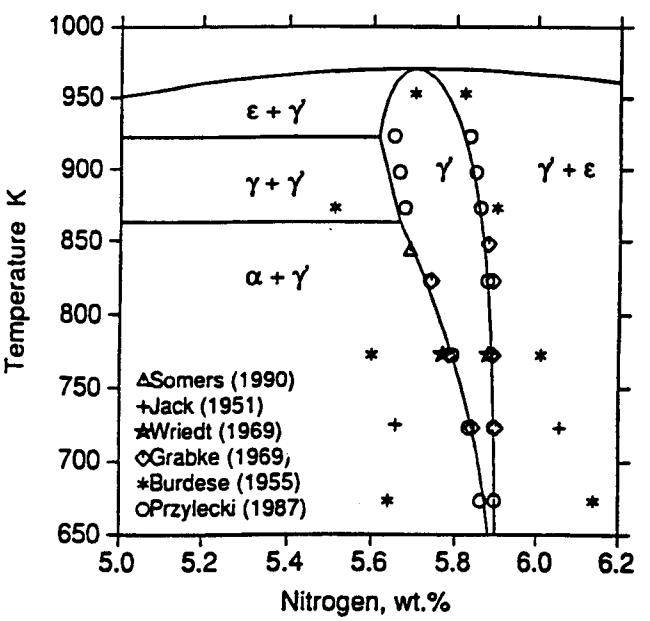

Fig. A2—Comparison between the calculated γ'-phase boundary of Fe-N[14] and experimental measurements.[17,18,29,37–39]

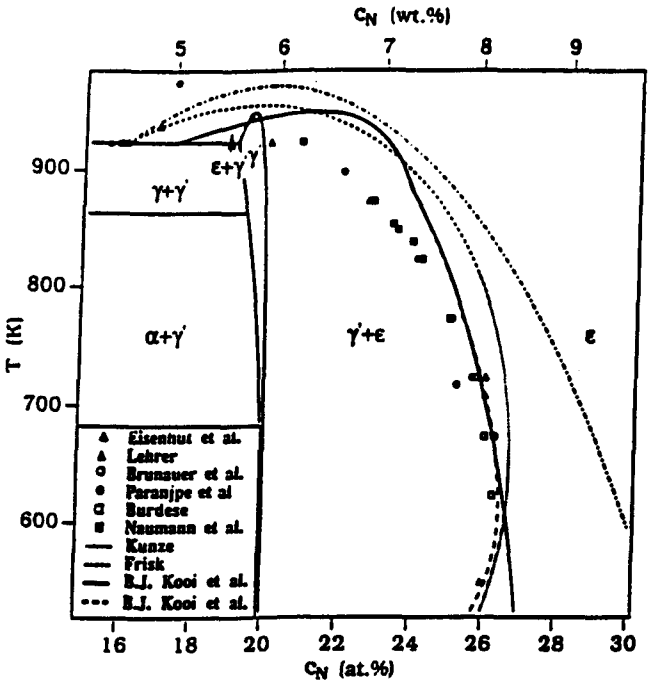

Fig. A3—Part of the Fe-N phase diagram, temperature T vs the nitrogen contents C_N, showing the $\gamma' + \varepsilon/\varepsilon$ phase boundary: Ref. 40—solid line and dashed line, Ref. 41—dotted line, Ref. 21—dash-dot line, and the corresponding experimental data.[15,16,42-45]

Table AII. Graphical Solution of Equations [17] and [18][7]*

	T (K)				
	823	833	843	848	853
C_N^S (wt pct)	—	—	8.50	—	—
$b_{\varepsilon\gamma'}$ (μm s$^{-1/2}$)	0.1310	0.1380	0.1450	0.1500	0.1540
b_ε (μm s$^{-1/2}$)	0.0565	0.0595	0.0635	0.0650	0.0665
$b_{\gamma'}$ (μm s$^{-1/2}$)	0.0745	0.0785	0.0815	0.0850	0.0875
$<D_N^{\gamma'}>$ (m^2 s^{-1}) $\times 10^{13}$	1.4610	1.6350	1.8240	1.9250	2.0300
$<D_N^{\varepsilon}>$ (m^2 s^{-1}) $\times 10^{14}$	2.4690	2.8610	3.3920	3.6760	3.9790

*The terms b_ε, $b_{\gamma'}$, and $b_{\varepsilon\gamma'}$ are the parabolic growth constants dependent on the surface nitrogen concentration C_N^S and the phase compositions at the ε/γ' and γ'/α interfaces at a given temperature.

Table AIII. Calculated Relative Variation of the Surface Nitrogen Concentration and the ε and γ' Layer Thicknesses

	Relative Variation (Pct)	
Confidence Interval (Pct)	Thickness of Layer $(\lvert\Delta\lambda\rvert/\lambda^m) \times 100$	Surface Nitrogen Concentration $(\lvert\Delta C_N \rvert / C_N^m) \times 100$
95	6	3.40

ACKNOWLEDGMENTS

The work in the present article was initiated in October 1990 and was part of the thesis of one of the authors (LT), which was presented in June 1994 (Doctorat INPL, Ecole des Mines de Nancy). We wish to thank Professor E.J. Mittemeijer and Dr. M.A.J. Somers (Delft University of Technology) for their advice and valuable discussions during our friendly meetings.

REFERENCES

1. T. Bell: *Heat Treat. Met.*, 1975, vol. 2, pp. 39-49.
2. H.J. Grabke: *Ber. Bunsenges. Phys. Chem.*, 1968, vol. 72, pp. 533-48.
3. H.J. Grabke: *Chemical Metallurgy of Iron and Steel*, Proc. Sheffield Conf., 1971, pp. 363-66.
4. H.J. Grabke: *Arch. Eisenhüttenwes.*, 1975, vol. 46, pp. 75-81.
5. H.J. Grabke: *Mater. Sci. Forum*, 1994, vol. 154, pp. 69-86.
6. R.E.E. Pulkkinen: *Met. Sci.*, 1982, vol. 16, pp. 37-40.
7. L. Torchane: Ph.D. Thesis, INPL, Nancy, France, 1994.
8. L. Torchane, P. Bilger, J. Dulcy, and M. Gantois: *Mater. Sci. Forum*, 1994, vols. 163–165, pp. 707-12.
9. M. Gantois: *Mater. Sci. Forum*, 1994, vols. 163–165, pp. 37-48.
10. M.A.J. Somers, and E.J. Mittemeijer: *Metall. Mater. Trans. A*, 1995, vol. 29A, pp. 57-74.
11. H. Du: Ph.D. Thesis, *Royal Institute of Technology*, Stockholm, Sweden, 1994.
12. B. Prenosil: *Konove Mater.*, 1965, vol. 3, pp. 69-87.
13. Yu.M. Lakhtin and Ya.D. Kogan: *Nitriding of Steel*, Mashinostroenie, Moscow, 1976 [(in Russian).]
14. H. Du: *J. Phase Equil.*, 1993, vol. 14 (6), pp. 682-93.
15. E. Lehrer: *Z. Electrochem.*, 1930, vol. 36, pp. 383-92.
16. V.G. Paranjpe, M. Cohen, M.B. Bever, and C.F. Floe: *Trans. AIME, J. Met.*, 1950, vol. 188, pp. 261-67.
17. A. Burdese: *Metallurgia Italiana*, 1955, vol. 47, pp. 357-66.
18. K.H. Jack: *Proc. R. Soc. A*, 1951, vol. 208, pp. 200-15.
19. D. Atkinson and C. Bodsworth: *J. Iron Steel Inst.*, 1970, vol. 208, pp. 587-93.
20. Z. Przylecki: *Sesja Naukowa Kom. Technol. Budowy Maszyn*, Poznan, 1979, pp. 35-84.
21. K. Frisk: CALPHAD, 1991, vol. 15 (1), pp. 79-106.
22. D. Heger and D. Bergner: *Härterei-Tech. Mitt.*, 1990, vol. 46, pp. 331-38.
23. K. Schwerdtfeger, P. Grieveson, and E.T. Turkdogan: *Trans. AIME*, 1969, vol. 245, pp. 2461-66.
24. L.S. Darken: *Trans. AIME*, 1948, vol. 175, pp. 184-94.
25. H. Du and J. Agren: *Mater. Sci. Forum*, 1992, vols. 102–104, pp. 243-48.
26. A. Marciniak: *Surf. Eng.*, 1985, vol. 1 (4), pp. 283-88.
27. Y. Adda and J. Phillibert: *La Diffusion Dans les Solides*, Tome I, Bibliothèque de Science et Technique Nucléaire, Saclay, France, 1966.
28. J. Crank: *The Mathematics of Diffusion*, Clarendon Press, Oxford, United Kingdom, 1956.
29. Z. Przylecki and L. Maldzinski: *Carbides, Nitrides, and Borides*, Poznan/Kolobrzeg, Poznan, Poland, 1987, pp. 153-62.
30. J. Slycke and L. Sproge: *Surf. Eng.*, 1989, vol. 5 (2), pp. 125-40.
31. M.A.J. Somers and E.J. Mittemeijer: *Mater. Sci. Forum*, 1992, vols. 102–104, pp. 223-28.
32. L.J. Dijkstra: *Trans. AIME*, 1949, vol. 185, pp. 252-60.
33. J.D. Fast and M.B. Varrijp: *J. Iron Steel Inst.*, 1955, vol. 180, pp. 337-43.
34. N.S. Corney and E.T. Turkdogan: *J. Iron Steel Inst.*, 1955, vol. 180, pp. 344-48.
35. W. Pitsch and E. Houdremont: *Arch. Eisenhüttenwes.*, 1956, vol. 27, pp. 281-84.
36. R. Rawlings and D. Tambini: *J. Iron Steel Inst.*, 1956, vol. 184, pp. 302-08.
37. H.J. Grabke: *Ber. Bunsenges. Phys. Chem.*, 1969, vol. 73, pp. 596-601 (in German).
38. M.A.J. Somers, N.M. Van Der Pers, D. Schalkoord, and E.J. Mittemeijer: *Metall. Trans. A*, 1990, vol. 21A, pp. 189-204.
39. H.A. Wriedt: *Trans. TMS-AIME*, 1969, vol. 245, pp. 43-46.
40. B.J. Kooi: Ph.D. Thesis, Delft University of Technology, 1995.
41. J. Kunze: *Nitrogen and Carbon in Iron and Steels; Thermodynamics*, Physical Research, Vol. 16, Akademie-Verlag, Berlin, 1990.
42. O. Eisenhut and E. Kaupp: *Z. Elektrochem.*, 1930, vol. 36 (6), pp. 392-404.
43. S. Brunauer, M.E. Jefferson, P.H. Emmett, and S.B. Hendricks: *J. Am. Chem. Soc.*, 1931, vol. 53, pp. 1778-86.
44. A. Burdese: *Ann. Chim.*, 1959, vol. 49, pp. 1873-84.
45. F.K. Naumann and G. Langenscheid: *Arch. Eisenhüttenwes.*, 1965, vol. 36 (9), pp. 677-82.